Int. J. Electrochem. Sci., 17 **(2022)** Article Number: 220530, doi: 10.20964/2022.05.35

International Journal of
ELECTROCHEMICAL
SCIENCE
www.electrochemsci.org

Short Communication

Electrochemical Synthesis of Ni-SnO_2 Composite Electrodes for Hydrogen Evolution Reaction in Alkaline Solution

Le-Hong Xing[*], *Xin-Ting Shi, Yi-Xin Wang, Li Zhang, Xiao-Yan Xu, Fan-Xu Meng, Jing Li*

Heilongjiang Key Laboratory of Photoelectric Functional Materials, College of Chemistry and Chemical Engineering, Mudanjiang Normal University, Mudanjiang 157011, China
[*]E-mail: xinglehonghit@163.com

Received: 28 January 2022 / *Accepted:* 1 March 2022 / *Published:* 5 April 2022

In this work, high efficient Ni-SnO_2 electrodes were prepared for the alkaline hydrogen evolution reaction (HER) by a simple composite electroplating method from sulphamate bath containing SnO_2 nano-particles. The Ni-SnO_2 electrode was physically characterized by scanning electron microscopy (SEM), energy dispersive analysis of X-ray (EDAX), and X-ray diffraction (XRD). These physical characterization results revealed that the homemade SnO_2 particles (about 170 nm) were successfully co-deposited in coatings. The composited SnO_2 changed the surface morphology and phase structure of Ni matrix. The electrochemical activities and stabilities for HER were monitored by steady-state polarization, Tafel plots, electrochemical impedance spectroscopy (EIS) and chronopotentiometry technique. The activity was confirmed via the quantification of H_2 gases that evolved during chronopotentiometry study. The Ni-SnO_2 showed a higher catalytic activity for H_2 evolution, compared with Ni. The OH_{ads} on SnO_2 surface was benefit to the formation of adsorbed H_{ads} which is the rate-determining step for HER.

Keywords: Hydrogen evolution reaction; Electro-catalysis; Composite electroplating; Ni-SnO_2

1. INTRODUCTION

With the economic development and progress of industry, the energy crisis and environmental pollution have caused the global concern [1]. Driven by the growing concern, efforts have been made to develop new environmentally friendly energy sources. Hydrogen (H_2) is identified as the most potential energy carrier in future for its clean, renewable and high efficient characters [2,3]. Water is the cheapest and most rich resources of hydrogen, and water electrolysis is a sustainable and promising method for hydrogen production [4,5]. The development of the higher activity electrode materials is particularly important for water electrolysis. Nickel-based materials, such as Ni and Ni-M alloys, are prominent non-noble metal catalysts for their good electro-catalytic activity for HER and

sufficient corrosion resistance in alkaline solution [6-10]. Recently, Ni-based metallic oxide composite material has received considerable attention because it exhibits a number of advantages. For example, Zheng et. al. [11] investigated the effect of CeO_2 particles in Ni coatings on the activity of HER. The results show that the Ni based CeO_2 electrodes show higher HER activity and better stability than pure Ni. H_{ads} can easily adsorb on Ce atoms due to the presence of several half-filled and empty d orbitals. Kullaiah et. al. [12] prepared Ni-TiO_2 electrode by composite electroplating method. The addition of TiO_2 is benefit to the formation of tiny nickel grains and increased the number of active site. Besides CeO_2 and TiO_2, a lot of metallic oxides such as ZnO [13], Cu_2O [14], and MoO_2 [15] have been used as co-catalyst to enhance the activity of HER on Ni based materials. However, the effects of SnO_2 nano particles addition on the performance of HER have not been fully investigated yet. SnO_2 is considered to be an excellent co-catalyst for methanol oxidation, ethanol oxidation and O_2 reduction in fuel cells [16-18]. It is very stable in alkaline solutions, and can support sufficient OH_{ads} species. The OH_{ads} is benefit to the formation of adsorbed H_{ads} [19]. The catalytic activity can be enhanced when the formation of adsorbed H_{ads} is the rate-determining step for HER (Volmer step). According to the well known "volcano" curve, the strength of Ni-H bond is relatively weak, and the formation of H_{ads} is always the rate-determining step for HER (Volmer step) on Ni electrode [20]. In this study, the aim of work is to utilize SnO_2 to enhance the HER activity of Ni coating electrode. We first synthesized SnO_2 nano-particles by hydrolysis method. And then, these SnO_2 particles were suspended in nickel plating solution. The Ni-SnO_2 composite coating was prepared by composite electrodeposited method. Multiple physical and electrochemical tests were employed to investigate the effect of SnO_2 particles embed in Ni coating on the activity of HER.

2. EXPERIMENTAL

2.1. Preparation of Ni-SnO_2 electrode

Preparation of SnO_2 Nanoparticles: 5-hydrated tin tetrachloride ($SnCl_4 \cdot 5H_2O$), sodium hydroxide, and ethanol were used as received without further purification. A sample of 17.53 g of $SnCl_4 \cdot 5H_2O$ was dissolved in 50 ml ultrapure water (18.2 M Ω cm, Mill-Q Corp.). The pH value of the solution was adjusted to 7 with NaOH solution. Then, the solution was transferred into a stainless steel reactor (100 ml). The reactor was put in an electric oven and kept at 160 ℃ for 2 h. After cooling to room temperature, the obtained product was separated by centrifugation. The resulting powders were washed in sequence with ethanoic acid - ammonium acetate solution and pure ethanol, and then dried at 80 ℃ for 12 h in vacuum. The particle size of homemade SnO_2 was about 200 nm.

Preparation of Ni-SnO_2 composite electrode: The Ni-SnO_2 composite electrode was electrodeposited on 4×5 cm copper sheet by composite electrodeposition method. The plating electrolyte was composed of 350 $g \cdot L^{-1}$ Ni $(NH_2SO_3)_2 \cdot 4H_2O$, 10 $g \cdot L^{-1}$ $NiCl_2 \cdot 6H_2O$, 30 $g \cdot L^{-1}$ NH_4Cl and various different content of SnO_2 nanoparticles. These composite electrodes were named as Ni/SnO_2-1, Ni/SnO_2-2, Ni/SnO_2-3, Ni/SnO_2-4, which were obtained from the above electrolyte with 1 $g \cdot L^{-1}$, 2 $g \cdot L^{-1}$, 3 $g \cdot L^{-1}$, 4 $g \cdot L^{-1}$ SnO_2 nanoparticles, respectively. The composite electrodeposition was carried out at

a current density of 3 A/dm^2, a temperature of 35 ℃ with a magnetic stirring at 850 rpm for 30 min.

2.2. Physical characterization

The morphology, crystal structure and the composition of the composite coatings were determined by SEM (Quanta 400, FEI), XRD (D8 Advance, Bruker) and EDAX, respectively.

2.3. Electrochemical measurements

Electrochemical studies including steady-state polarization, tafel plots, EIS and amperometric current density-time curves of the composite electrodes were conducted using electrochemical working station (PARSTAT 4000) in a standard three-electrode cell in 1 M NaOH solution. The composite electrodes were used as working electrode and 1 cm^2 platinum foil was served as counter electrode. Hg/HgO electrode was used as the reference electrode. The scan rate of steady-state polarization test was 5 mV·s^{-1}. The EIS was measured at -0.125 V (vs. SCE) in a frequency range from 100 kHz to 0.01 Hz with 6 – 12 points per decade. The amplitude of the AC-voltage was 0.005 V. All the electrochemical measurements were carried out at 25 ^{o}C.

3. RESULTS AND DISCUSSION

Fig. 1 is the IR spectra of homemade SnO_2 nanoparticles. The characteristic peak in the range of 500-750 cm^{-1}, 1600 cm^{-1}, and 3430 cm^{-1} are assigned to Sn-O vibration, O-H bending vibration and O-H stretching vibration [16]. SnO_2 in composite electrodes can support abundant OH_{ads} species which are benefit to the formation of adsorbed H_{ads} during HER [21]. Fig. 2 is XRD patterns of SnO_2 nanoparticles. The SnO_2 nanoparticles show the major diffraction peaks of (110), (101), (111), (211), (301) and (321) [22]. The average size of SnO_2 particles were calculated from the most intense peak (110) according to Sherrer's Equation [23]. The particle size of SnO_2 was about 170 nm .

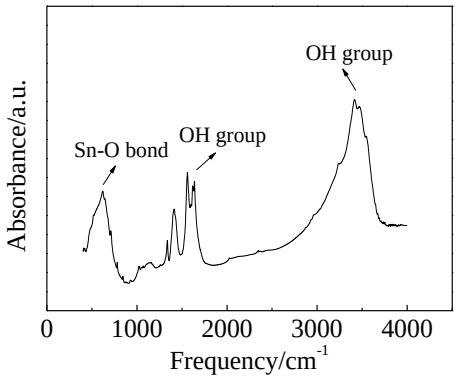

Figure 1. FTIR plot of homemade SnO_2 particles after dehydration treatment at 200 ^{o}C under vacuum condition.

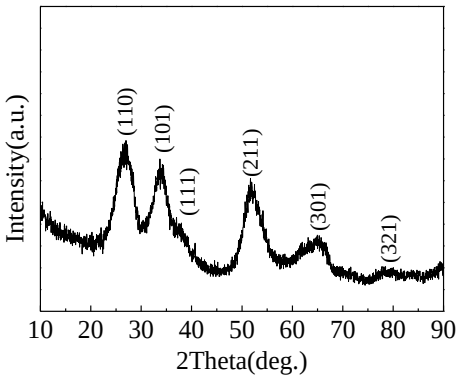

Figure 2. XRD analysis of SnO_2 nanoparticles.

The XRD patterns of Ni and Ni/SnO_2-3 electrodes are shown in Fig.3. The diffraction peaks for the two electrodes at 2θ about 44.5°, 51.8° and 76.4° can be attributed to Ni (111), Ni (200) and Ni (220). The peaks for Ni/SnO_2-3 electrode at about 26.6°, 33.8°, 38.7°, 51.7° and 54.3° can be well indexed to SnO_2 (JCPDS:41-1445). SnO_2 particles were successfully co-deposited in Ni matrix. The preferential orientation of Ni electrode is (200) crystal plane. The preferential orientation of Ni/SnO_2-3 electrode has been greatly changed to (111) crystal plane. Ni (111) plane was more benefit to the enhancement of electrocatalytic performance for HER than other planes [24,25]. The full width of half maximum values of Ni (111) and Ni (200) for pure Ni electrode is 0.193° and 0.233°, respectively. The two values for Ni/SnO_2-3 electrode are 0.204°and 0.303°, respectively. The diffraction peaks of Ni/SnO_2-3 electrode are broader than Ni. According to Sherrer's Equation, the crystallite size of composite electrode is smaller than that of Ni. The co-deposition of SnO_2 particles in Ni matrix has the effect of grain refinement.

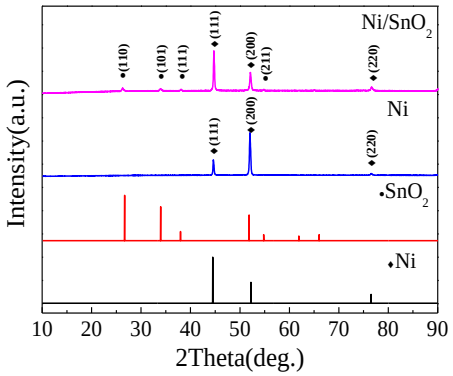

Figure 3. XRD patterns of Ni and Ni/SnO_2-3 electrodes.

SEM images of Ni and Ni/SnO_2 electrodes are shown in Fig.4. As shown in Fig.4(a) and (b), The Ni electrode shows a relatively bulky microstructure. The co-deposition of SnO_2 nano-particles makes the coating crystallization more meticulous and porous, which is benefit to increase of surface area. The white spherical particles in Fig.4(b) are SnO_2. The mean size of SnO_2 nano-particles is about

200 nm, which is consistent with the above XRD results. The presence of SnO_2 nano-particles in the composite electrode is confirmed via EDAX analysis. The amount of SnO_2 nano-particles incorporated in Ni/SnO_2-3 is approximately 4.7 wt%.

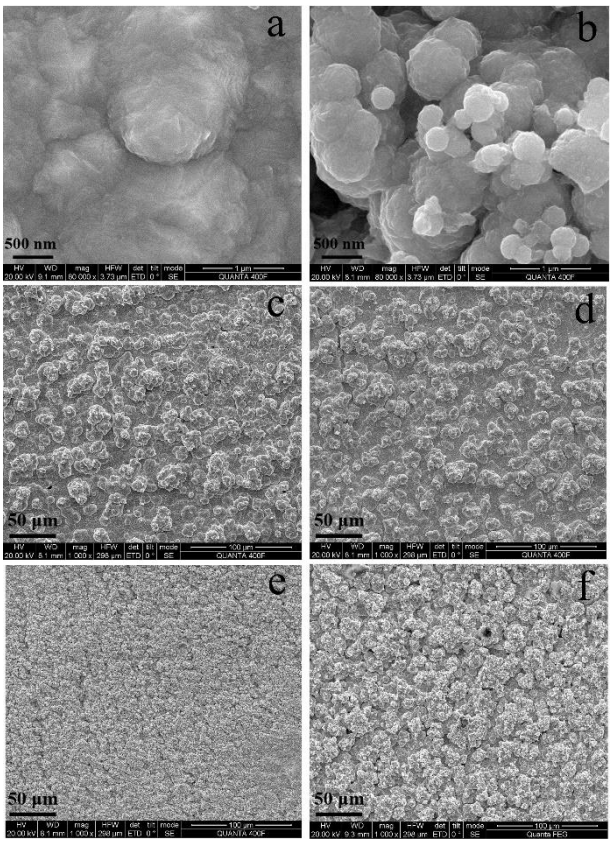

Figure 4. Low and high-magnification SEM images of electrode: (a) magnified Ni; (b) magnified Ni/SnO_2-3; (c) Ni/SnO_2-1; (d) Ni/SnO_2-2; (e) Ni/SnO_2-3; (f) Ni/SnO_2-4.

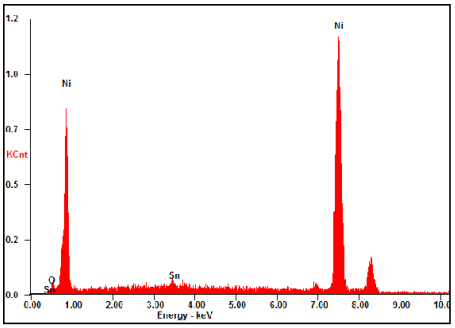

Element	Wt%	At%
OK	01.62	05.81
SnL	03.04	01.47
NiK	95.33	92.72
Matrix	Correction	ZAF

Figure 5. EDAX patterns of Ni/SnO_2-3 composite electrode and its quantitative analysis.

The electrocatalytic activity for HER on Ni/SnO_2 composite electrodes are tested by a series of electrochemical measures including cathode polarization curves, Tafel plots, and EIS. The corresponding parameters obtained from above electrochemical measurements are listed in Table 1.

Fig.6 (a) shows the cathode polarization curves of different electrodes. It is apparent that Ni/SnO_2-3 shows the highest catalytic activity, which demand the lowest overpotential of 427 mV to drive current densities of 10 mA cm^{-2}.

To further understand the mechanism of the HER, the Tafel plots in Fig.6 (b) are fitted to the classic Tafel equation (Eq. 1). The values of R^2 are greater than 0.99, which indicate that the calculated kinetic parameters listed in Table 1 adjust well to Tafel equation.

$$\eta = b\ log(j/j_0) \quad (1)$$

Here η is the cathode overpotential, b is the Tafel slope, j is current density and j_0 is the exchange current density. The j_0 in Table 1 represents the HER catalytic activity of the electrodes. As shown in Table 1, the j_0 values of these Ni/SnO_2 electrodes are all higher than that of pure Ni electrode. With the increase of the SnO_2 content in coatings, the values of j_0 for Ni/SnO_2 electrodes are first enhanced and then tend to decline. The catalytic activity of Ni/SnO_2-3 obtained from electrolyte with 3 $g \cdot L^{-1}$ SnO_2 nano-particles is the highest. The co-deposition of SnO_2 particles makes the grain size of the composite coating much finer than that of pure nickel. This fining effect is beneficial for HER. Too much SnO_2 co-deposit in the composite electrode may affect the electrode activity for its low electron conductivity. Tafel slope b is a significant parameter which can indicate the dominant HER mechanism on electrodes. As shown in Fig. 6(b) and Table 1, the b of the Ni and these Ni/SnO_2 composite electrodes are 120, 204, 199, 187 and 205 $mV \cdot dec^{-1}$, respectively. According to the reported literature [26-29], the rate-determining steps of HER on above studied electrodes are Volmer reaction. The formation of H_{ads} determines Volmer reaction rate. SnO_2 in composite electrodes can support abundant OH_{ads} species. These OH_{ads} species can promote H_2O decomposition and H_{ads} formation by weakening the oxophilicity of the active site [30,31]. The SnO_2 and Ni interface benefits for the H_{ads} adsorption, but suppress the competitive H_2O_{ads} and OH_{ads} adsorption [32]. Hence, the Ni-SnO_2 showed a higher catalytic activity for H_2 evolution, compared with Ni.

The EIS measurements are carried out on Ni and Ni/SnO_2 electrodes at cathode potential of -0.125 V (vs. SCE) under HER operating conditions. The Nyquist diagrams are illustrated in Fig.6 (c). A widely used equivalent circuit is used to describe the HER process and the fitting results of the resistance elements are listed in Table1. The ohmic resistances (R_s) of these composite electrodes are all higher than that of Ni. SnO_2 co-deposit in the composite electrodes decrease the electron conductivity of electrode. The electrochemical reaction resistance (R_{ct}) of Ni/SnO_2-3 electrode is the lowest among all of studied electrodes. The bode phase angle plot obtained for these composite electrodes are presented in Fig.6 (d). All these plots abide by one-time-constant behavior, which is in good agreement with above mentioned equivalent circuits model given in Fig.6 (c). Also, the Ni/SnO_2-3 electrode has the lowest phase angle and impedance value, which confirms the enhanced HER rate.

The SnO_2 co-deposit in Ni electrodes can accelerate the HER process. Excessive SnO_2 in the composite electrodes decrease HER activity for the low electron conductivity of electrode. The Ni/SnO_2-3 with the optimal addition of SnO_2 in Ni shows the highest catalytic activity, which is coincident with the results of steady-state polarization in Fig.6 (a) and Tafel plots in Fig. 6 (b). C_{dl} is double layer capacitance which is associated with surface area of electrode [33,34]. The addition of SnO_2 raises the value of C_{dl}, which indicates that surface area of composite electrode has been increased. SnO_2 makes the Ni coating crystallization more tiny. The increase of active surface area

benefits for the formation of H_{ads}. This experimental finding is consistent with above SEM results.

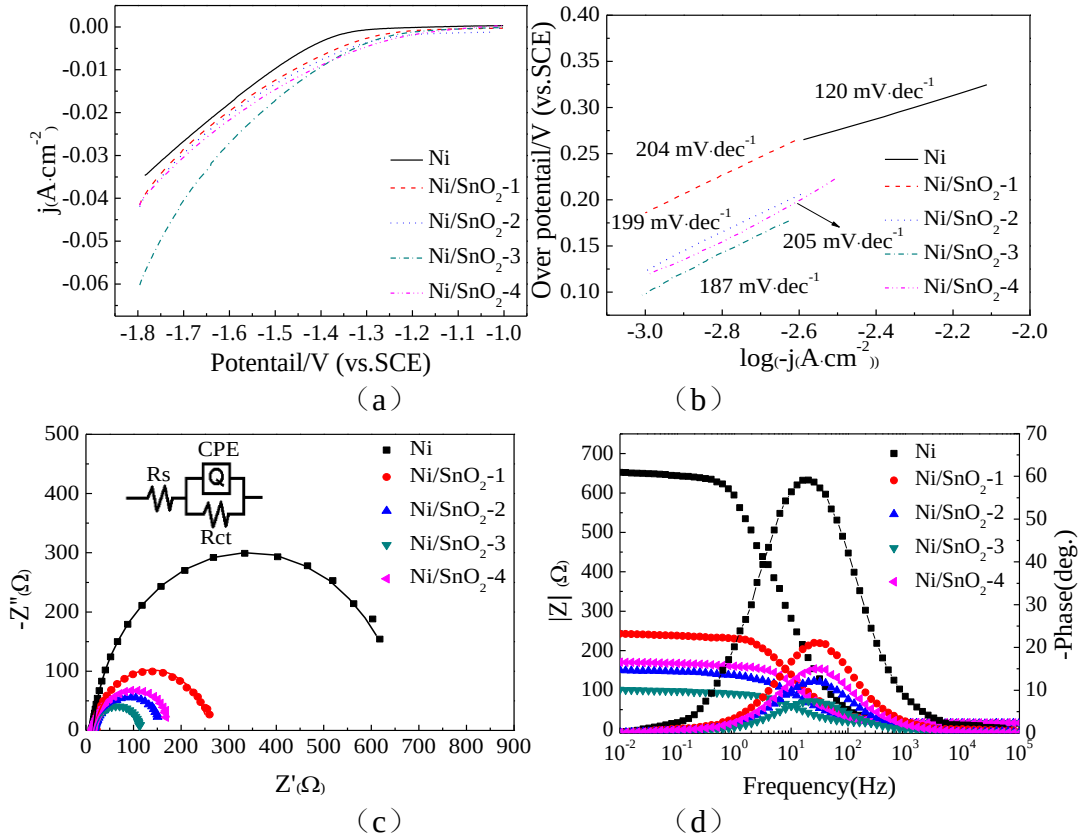

Figure 6. Electrochemical properties for HER on Ni and Ni/SnO_2 composite electrodes in 1 M NaOH. (a) Steady-state polarization curves, (b) Corresponding Tafel plots, (c) Nyquist diagrams (dots) and fitting diagrams (lines) based on possible equivalent circuits, (d) Bode plots.

Table 1. Electrocatalytic parameters obtained from above electrochemical measurements in 1 M NaOH solution.

	j_o ($uA \cdot cm^{-2}$)	b ($mV \cdot dec^{-1}$)	η_{10} (mV)	R_s (Ω)	R_{ct} (Ω)	C_{dl} (10^{-5} $F \cdot cm^{-2}$)
Ni	0.673	120	501	14.7	652.7	8.17
Ni/SnO_2-1	22.57	204	540	14.8	240.5	14.32
Ni/SnO_2-2	37.51	199	483	15.4	149.7	21.73
Ni/SnO_2-3	52.29	187	427	15.8	100.6	26.31
Ni/SnO_2-4	39.21	205	493	16.6	168.8	19.77

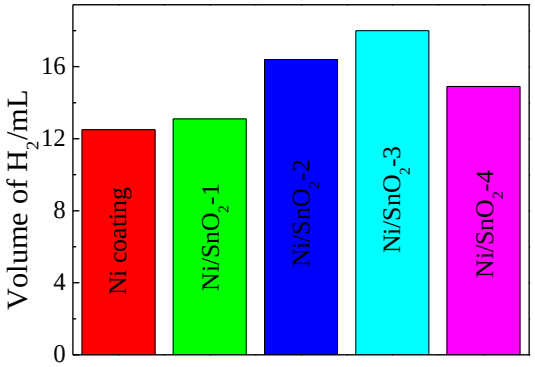

Figure 7. The volume of H_2 evolved on each studied electrode at cathode current density of 300 mA·cm^{-2} for 300 s

Fig. 7 shows the volume of H_2 gas evolved on each studied electrode for 300 s at a constant cathode current density of 300 mA·cm^{-2}. The Ni/SnO_2-3 electrode obtained from the electrolyte with 3 g·L^{-1} SnO_2 particles produces the maximum amount of H_2 (17.9 mL) compared to the other coatings. This result confirms that the Ni/SnO_2-3 shows the best activity for HER.

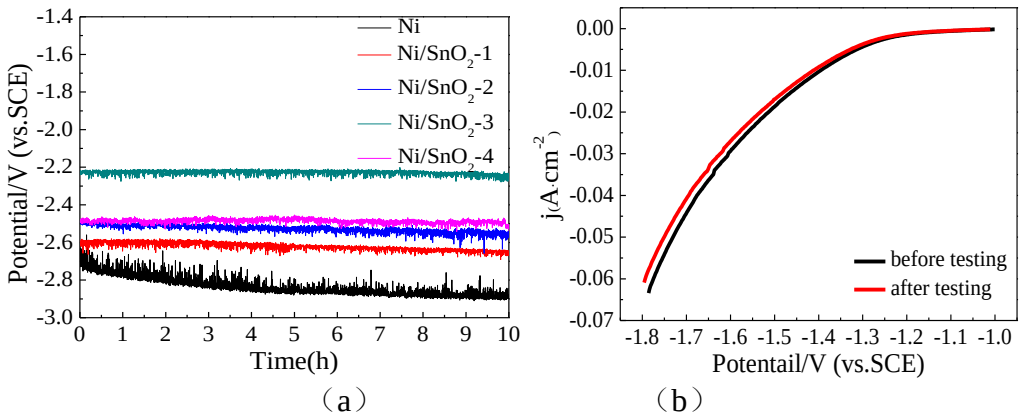

Figure 8. Stability tests of the composite electrodes. (a) The chronopotentiometry study at cathode current density of 100 mA·cm^{-2}, (b) Polarization curves of Ni/SnO_2-3 before and after 10 h chronopotentiometry test in 1 M NaOH solution.

The behavior of the electrode potential as a function of time at cathode current density of 100 mA·cm^{-2} is shown in Fig.8. The decrease of electrode potential for Ni, Ni/SnO_2-1, Ni/SnO_2-2, Ni/SnO_2-3, and Ni/SnO_2-4 is 323 mV, 54 mV, 101 mV, 34 mV and 49 mV, respectively. The HER stability of the composite electrode are all higher than pure Ni. The polarization curves of Ni/SnO_2-3 before and after 10 h stability test show negligible changes. The Ni/SnO_2-3 electrode demonstrates excellent stability.

The electrochemical properties of Ni/SnO_2 are compared with other composite materials reported in literatures. The comparison of these works is listed in Table 2. As shown in Table 2, the Ni/SnO_2 exhibits lower over potential [35-37] and higher exchange current density [38,39]. The

performance of hydrogen evolution with Ni/SnO_2 electrode catalyst is obvious higher than other reported composited materials.

Table 2. The activity of HER on different composite electrodes reported in literatures and this work

Electrode	Alkaline solution	*b* (mV·dec^{-1})	η (mV)	j_0 (uA·cm^{-2})	Reference
Ni/SnO_2	1 M NaOH	187	427 (η_{10})	52.29	this work
Ni-Sn@C PNs	1 M NaOH	145	1230 (η_4)	-	[35]
(Ni-MoS_2)$_{1000}$	2mM $HClO_4$/ 0.1 M $NaClO_4$	120	680 ($\eta_{0.35}$)	8×10^{-4}	[36]
Cu/Cu_2O/ Ni NP	0.1 M H_2SO_4	50	456 (η_{10})	-	[37]
Ni-PAni	4 M KOH	-	-	3.47	[38]
Ni/WO_3	1 M KOH	124.7	-	5.88	[39]
Ni/Bi_2O_3	1 M KOH	128.8	-	2.29	[39]
Ni/SC	1 M KOH	116.9	-	2.43	[39]

4. CONCLUSIONS

The high efficient Ni-SnO_2 electrodes are fabricated by a simple low-cost composite electroplating method. Compared with pure Ni, the Ni/SnO_2 catalyst gives a higher catalytic activity and stability for HER. The co-deposition of SnO_2 in Ni coating makes metal crystallization finer and tinier, which increase the active surface area of electrode. The co-deposition of SnO_2 changes the preferential orientation of Ni to (111) crystal plane which is more benefit to the activity of HER. The OH_{ads} on SnO_2 surface facilitates the formation of adsorbed H_{ads} which is the rate-determining step for HER. SnO_2 is a promising co-catalyst to enhance the activity of HER on Ni based materials.

ACKNOWLEDGEMENT
This work was supported by the Mudanjiang Normal University Key Project (No. GP2021002), the Research Fund Project of Mudanjiang Science and Technology Project of Mudanjiang city (No. SQ2020JG115), the Teaching reform Projects of MuDanjiang Normal University (No. KCSZ-2020021), the Innovation Project of University Students (202110233043).

References

1. Y. Wu, R. Sun and J. Cen, *Front. Chem.*, 8 (2020) 386.
2. S. Wang, W. Li, H. Qin, L. Liu, Y. Chen and Di. Xiang, *Int. J. Electrochem. Sci.*, 14 (2019) 957.
3. S.J. Gutić, M. Šabanović, D. Metarapi, I.A. Pašti, F. Korać and S.V. Mentus, *Int. J. Electrochem. Sci.*, 14 (2019) 8532.
4. H. Wang and L. Gao, *Curr Opin Electrochem.*, 7 (2018) 7.
5. S. Feng, R. Xu, X. Wang, W. Wang, C. Chen and A. Ju, *Int. J. Electrochem. Sci.*, 15 (2020) 2806.
6. L. Zu, J. He, X. Liu, L. Zhang and K. Zhou, *Int. J. Hydrog. Energy*, 44 (2019) 4650.
7. Y. Wu and H. He, *Int. J. Hydrog. Energy*, 43 (2018) 1989.
8. X. Zhang, L. Yi, Y. Guo, A. Hu, M. Li, T. Huang and H. Ling, *Int. J. Hydrog. Energy*, 44 (2019) 29946.
9. X. Yin, H. Dong, G. Sun, Wu. Y, A. Song, Q. Du, L. Su and G. Shao, *Int. J. Hydrog. Energy*, 42 (2017) 11262.
10. L. Wang, Y. Li, X. Yin , Y. Wang, L. Lu, A. Song, M. X., Z. Li., X. Q and G. Shao, *Int. J. Hydrog. Energy*, 42 (2017) 22655.
11. Z. Zheng, N. Li, C. Wang, De. Li, Y. Zhu and G. W, *Int. J. Hydrog. Energy*, 37 (2012) 13921.
12. R. Kullaiah, L. Elias and A.C. Hegde, *Int. J. Miner. Metall. Mater.*, 25 (2018) 472.
13. N. Wang, B. Tao, F. Miao and Y. Zang, *RSC Advances*, 9 (2019) 33814.
14. N. Farahbakhsh and S. Sanjabi, *J Ind Eng Chem.*, 70 (2019) 211.
15. B. Ren, D. Li, Q. Jin, H. Cui and C. Wang, *J. Mater. Chem. A*, 10 (2017) 1.
16. L. Xing, *Int. J. Electrochem. Sc.i*, 15 (2020) 2375.
17. H. Gharibi, S. Sadeghi and F. Golmohammadi, *Electrochim. Acta*, 190 (2016) 1100.
18. N. Zhang, L. Du, C. Du and G. Yin, *RSC Adv.*, 6 (2016) 26323.
19. J.A.S.B. Cardoso, B. Šljukić, E. Kayhan and C.A.C. Sequeira, *Catal. Today*, 357 (2020) 302.
20. A. Lasia, *Handbook of fuel cells*, 815 (2010) 1.
21. L. Cai, Z. Lin, M. Wang, F. Pan, J. Chen, Y. Wang, X. Shen and Y. Chai, *J. Mater. Chem. A*, 5 (2017) 24091.
22. X. Zhou, W. Fu, H. Yang, D. Ma, J. Cao, Y. Leng, J. Guo, Y. Zhang, Y. Sui, W. Zhao and M. Li, *Mater. Chem. Phys.*, 124 (2010) 614.
23. Y. Pan, Z. Guo, T. Guo, X. Wang and J. Huang, *Surf. Coat. Technol.*, 298 (2016) 33.
24. W. Zhen, J. Ma and G. Lu, *Appl. Catal. B*, 190 (2016) 12.
25. L. Wang, Y. Li, X. Yin, Y. Wang, A. Song, Z. Ma, X. Qin and G. Shao, *ACS Sustain. Chem. Eng.*, 5 (2017) 7993.
26. G. Zhao, K. Rui, S. Dou and W. Sun, *Adv. Funct. Mater.*, 28 (2018) 1803291.
27. A. Lasia, *Int. J. Hydrog. Energy*, 44 (2019) 19484.
28. L. Zhang, Y. Zheng, J. Wang, Y. Geng, B. Zhang, J. He, J. Xue, T. Frauenheim and M. Li, *Small*, 17 (2021) 2006730.
29. Y. Bahari Mollamahale, N. Jafari and D. Hosseini, *Mater. Lett.*, 213 (2018) 15.
30. B. Mao, P. Sun, Y. Jiang, T. Meng, D. Guo, J. Qin and M. Cao, *Angew.Chem.*, 59 (2020) 15232.
31. P.F.B.D. Martinsa, P.P. Lopes, E.A. Ticianelli, V.R. Stamenkovic, N.M. Markovic and D. Strmcnik, *Electrochem commun.*, 100 (2019) 30.
32. L. Peng, X. Zheng, L. Li, L. Zhang, N. Yang, K. Xiong, H. Chen, J. Li and Z. Wei. *Appl. Catal. B*, 245 (2019) 122.
33. J. Wang, J. Chen, J. Chen, H. Zhu, M. Zhang and M. Du, *Adv. Mater. Interfaces*, 4 (2017) 1700005.
34. L. Song, X. Wang, F. Wen, L. Niu, X. Shi and J. Yan, *Int. J. Hydrogen Energy*, 41 (2016) 18942.
35. L. Lang, Y. Shi, J. Wang, F. Wang, and X. Xia, *ACS Appl. Mater. Interfaces*, 17 (2015) 9098.
36. D. Escalera-López, Y. Niu, J. Yin, K. Cooke, N.V. Rees and R.E. Palmer. *ACS Catal.*, 9 (2016) 6008.
37. N. Farahbakhsh and S. Sanjabi. *J. Ind. Eng. Chem.*, 70 (2019) 211.

38. C. Torres, B. Morenob, E. Chinarro and C. de Fraga Malfattic, *Int. J. Hydrog. Energy*, 32 (2017) 20410.
39. M.J. Gómez, V.B. Llorente, A. Hainer, G.I. Lacconi, J.C. Scaiano, E.A. Franceschini and A.E. Lantern, *Sustain. Energy Fuels*, 8 (2020) 3963.